

# Introduction of a reverse simulation approach to identify the fatigue SIF crack arrest threshold from fretting cracking experiments

Alix de Pannemaecker<sup>1&2,\*</sup>, Siegfried Fouvry<sup>1</sup>, Jean-Yves Buffière<sup>2</sup>

<sup>1</sup> LTDS, Ecole Centrale Lyon, 69134 Ecully, France

<sup>2</sup> MATEIS, INSA Lyon, 69100 Villeurbanne, France

\* Corresponding author: alix.de-pannemaecker@ec-lyon.fr

---

## Abstract

Fretting is a small amplitude oscillatory movement appearing between two contacting surfaces subjected to vibrations. This phenomenon may generate crack growth propagation. The aim of the present work is to estimate the  $\Delta K_{Ith}$  (Crack arrest stress intensity factor) related to the crack arrest condition of a material subjected to partial slip fretting loadings by coupling experimental results and numerical simulations. The study is limited to cylinder/plane models TA6V/Al-alloys. In this approach, fretting tests are first performed for each configuration to obtain the crack length as a function of fretting cycles in order to establish the length of the arrested crack. Then an automatic program based on FEM simulations of the experimental test is developed to estimate the stress intensity factor corresponding to the crack arrest. Using a reverse analysis, the  $\Delta K_{th}$  corresponding to the crack arrest condition is identified and different materials are compared.

**Keywords** Fretting tests, Fatigue crack arrest, Crack closing, Stress intensity factor

---

## 1. Introduction

Araujo et al. [1] demonstrated that the fretting fatigue endurance can be formalized using a short crack arrest methodology. This approach has been adopted in [2] to estimate the crack arrest boundary in the fretting fatigue map approach. Such analysis consists in computing the evolution of the stress intensity factor as a function of the crack length and to evaluate if this K-factor loading path intercepts or not the short crack arrest boundary. If the  $\Delta K$  loading path overpasses this boundary, then a fretting fatigue failure is expected. Note that the short crack arrest boundary is approximated using either KT or El Haddad formalism.

Such a methodology usually considers a crack localized at the contact border and perpendicular to the contact surface. However, experimental results show that the crack path below the interface is more complex and usually displays an oblique angle oriented toward the inner part of the contact. A major question is to know if the normal crack approximation is relevant to describe the real crack path evolution.

A second aspect concerns the short crack methodology which is usually applied to approximate the crack arrest condition. In this research work, we consider an original reverse approach which consists in estimating the  $\Delta K_{Ith}$  related to the studied material by applying a reverse identification method of our experimental results.

## 2. Materials and experimental procedure

### 2.1. Materials

A 2000 series al alloy (2196) aluminum alloy was investigated with the chemical composition detailed in Table 1.

Table 1. Chemical composition of the 2196 aluminum

% Cu	% Li	% Mg	% Mn	% Ag	% Zr	% Zn	% Si	% Fe
2.5-3.3	1.4-2.1	0.25-0.8	< 0.35	0.25-0.6	0.04-0.18	< 0.35	< 1.2	< 0.15

Two different heat treatments were applied: the industrial peak aged on one side called T8, and the experimental treatment at low temperature (120°C during 96 hours) on the other, called UA (Under-Aged). These two ageing treatments involve equivalent elastic properties with an elastic modulus  $E$  about 79000 MPa and the Poisson's coefficient about 0.305, but different monotonic and fatigue properties like the ultimate stress  $R_m$ , the yield stress  $R_{0.2}$  and the elongation's rate  $A\%$  (Table 2), which imply different  $\Delta K_{th}$  values. Note that for confidential reasons, all data regarding fatigue properties are not available.

Table 2. Mechanical properties of the 2196 aluminum, depending on the heat treatment

State	$R_{0.2}$ (MPa)	$R_m$ (MPa)	$A\%$
T8	559	594	5.9
UA	428	520	11.1

For each alloy, small cubic specimen were machined and polished to achieve a  $0.2 \mu m R_a$  roughness. Samples were adjusted so that the fretting loading was applied along the rolling direction of the alloy (Fig. 1).

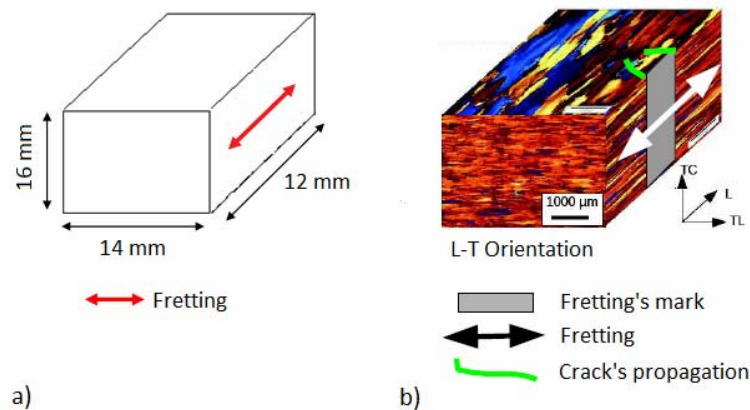


Figure 1. a) Sample's geometry - b) Microstructure [3]

### 2.2. Plain Fretting Experiment

Plain partial slip fretting tests were performed on a hydraulic set up at the LTDS previously described by Heredia [2]. The normal force ( $P$ ) is kept constant, while the tangential force ( $Q$ ) and displacement ( $\delta$ ) amplitudes are recorded. The fretting loop can be plotted and the corresponding amplitude values (respectively  $Q^*$  and  $\delta^*$ ) defined (Fig. 2).

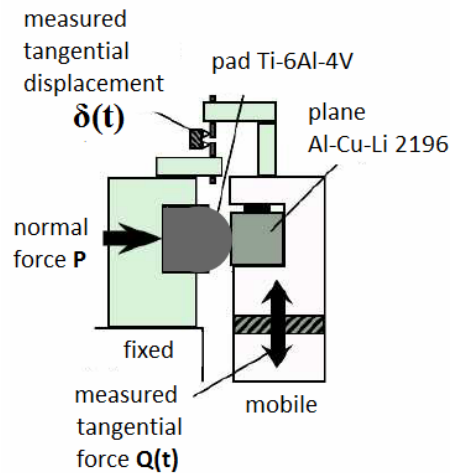


Figure 2. Experimental set up [2&3]

In the present fretting cracking investigation the displacement amplitude was monitored in order to maintain partial slip conditions, keeping constant the tangential force amplitude during the whole test duration. A cylinder/plane configuration was applied. The fretting pad consists of a Ti-6Al-4V alloy which displays the following elastic properties: 119500 MPa for the elastic modulus and 0.287 for the Poisson's coefficient. The cylinder's radius was fixed at 80 mm and the applied normal force at  $P=436.5$  N/mm which induces a maximum hertzian constant pressure  $p_0=300$  MPa and a hertzian constant radius  $a_H=0.92$  mm. The lateral width of the cylinder pad was about 8 mm which corresponds to plain strain conditions along the median axis of the fretting scar. Previous tests were done to determine the friction coefficient at the sliding transition  $\mu_t=0.85$ . [4]

### 3. Experimental results

Our objective was to identify the evolution of the crack length as a function of the fretting cycle to establish the "plateau" value related to the crack arrest condition. The tangential force was kept constant for all the experiment with  $Q^*=200$  N/mm. This tangential loading was previously adjusted to guarantee significant fretting cracking for elastic configurations (i.e. the stress is inferior to the yield stress  $R_{0.2}$ ).

Figure 3 shows a typical crack path observed for the studied configuration after  $2.10^6$  cycles. As usually observed the incipient crack propagation a near  $45^\circ$  orientation compared to the normal of the surface until about  $30 \mu\text{m}$  in depth. Below  $200 \mu\text{m}$ , the crack propagation direction is normal to the plan. Between  $30$  and  $200 \mu\text{m}$ , the crack path is considered to be linear with a  $10^\circ$  angle with respect to the normal of the surface. A schematic description of the crack path is given in Figure 3. The major part of the crack expertise leads to similar evolutions, so that the overall crack path description can be provided by linear segments (Fig. 3), and by making the average, we kept the first angle at  $47.5^\circ$ , the second at  $15.5$  and the last at  $0^\circ$  for the numerical model exposed hereafter.

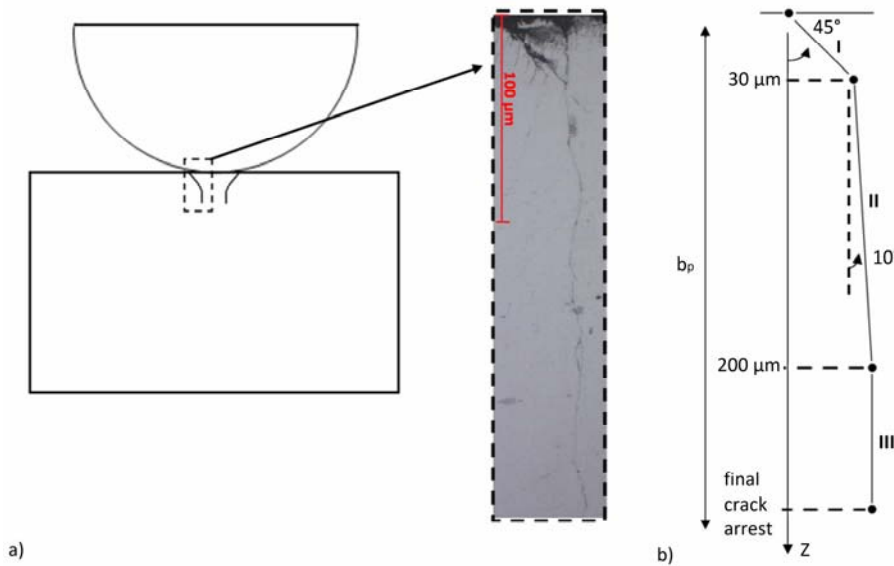


Figure 3. Crack path description a) Schematic and photo of the 2196-UA at  $N=2 \cdot 10^6$  - b) Discretization of the real crack path

This typical crack path evolution will be considered later for the crack modelling. To simplify the crack length analysis only the projected crack length ( $b_p$  parameter on Fig. 3) was considered. Figure 4 compares the evolution of the maximum projected crack length which was represented as a function of the fretting cycle.

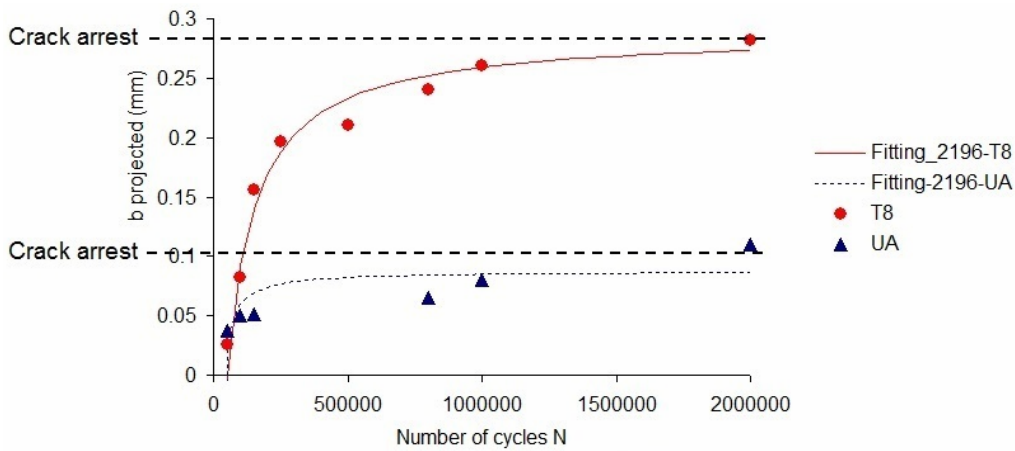


Figure 4. Propagation's curves

For the two materials, asymptotic evolutions can be observed. This analysis shows that the maximum crack length stabilized after  $10^6$  cycles. This allows us to estimate the crack length related to the crack arrest condition for the studied ( $P=436.5 \text{ N/mm}$ ;  $Q^*=200 \text{ N/mm}$ ) plain fretting condition. We found respectively for the T8 and UA ageing treatments the following  $b_{pth}(T8)=280 \text{ }\mu\text{m}$  and  $b_{pth}(UA)=100 \text{ }\mu\text{m}$  crack length values. Because the maximum crack length achieved for the T8-ageing is longer than the one observed for the UA-ageing, it can be intuited that the threshold Stress Intensity Factor (SIF) related to the T8-treatment is significantly smaller than the one expected for the UA-ageing. The following analysis will consist in quantifying this aspect.

## 4. FEM computation of the Stress Intensity Factor's (SIF) evolution below the fretting contact

### 4.1. Contact modeling

A 2D-plain strain FEM modeling of the studied plain fretting test was developed. All the elastic and friction properties previously defined during experiment tests were implemented in the FEM-model. The fretting model is composed of a fixed plane and a moving cylindrical pad (Fig. 5). The mesh is composed of triangular (CPE3) and quadratic (CPE4R) linear elements. Quadratic elements were used to define the crack tip zone in a round domain of a radius of  $5\mu\text{m}$ . Outside the crack tip zone, triangular elements were considered in order to reduce time costs. The mesh size in the contact zone was refined down to  $20\mu\text{m}$  in order to provide a more accurate estimation of the contact stress fields. The contact and the crack were described by a master-slave algorithm, and the tangential loading was determined by Lagrange multipliers through a constant friction coefficient ( $\mu_t=0.85$ ). During a computation, a fretting cycle were reproduced through the introduction of a normal load  $P=436.5\text{ N/mm}$  and through the application of a cyclic tangential cycle with a  $Q^*=200\text{ N/mm}$ .

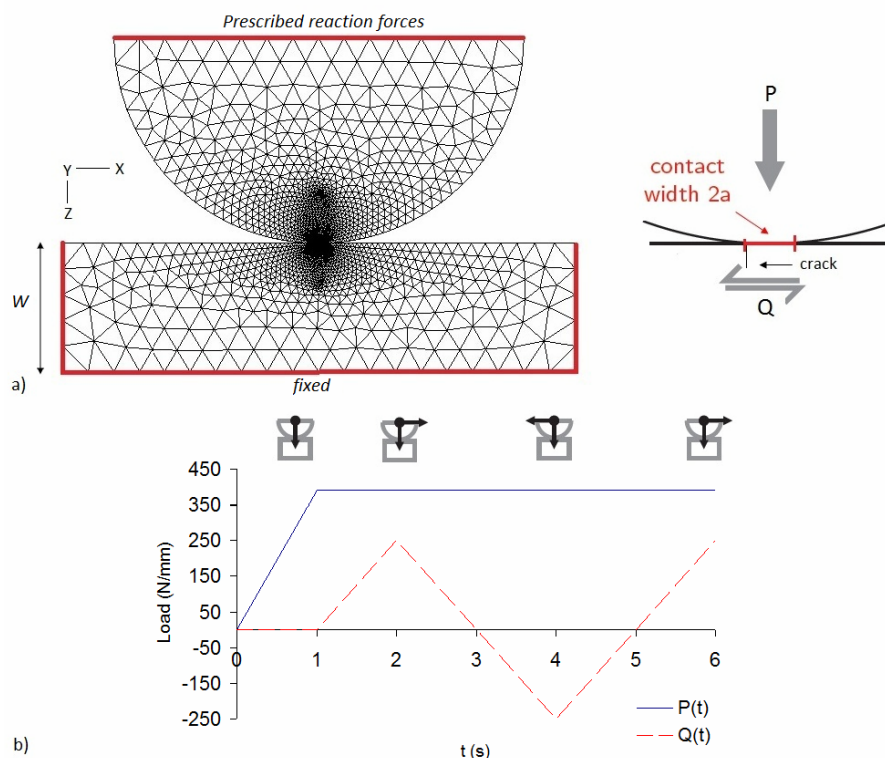


Figure 5. FEM description of the plain fretting cracking experiments a) FEM model - b) Loads applied

As elastic loads were imposed, the cracking computation was restricted to a single loading cycle. Results and interpretations were made for a single crack located at the trailing contact border ( $x=-a_H$ ) at the loading stage ( $Q=Q^*$ ) which infers an open crack condition (Fig. 5).

## 4.2. Computation of the SIF parameter, crack meshing

An automatic Matlab code was developed to generate Abaqus input scripts, which remesh the cracks in a fretting cylinder/plane interface during the propagation's stage. This model with its mesh was inspired by the work of H. Proudhon [5]. The crack patch can be located anywhere in the plane's interface and can be described using sequential segments to reproduce as close as possible the real crack path. In the present investigation, crack nucleation is located at the contact border which is confirmed by experimental observations and multiaxial fatigue Modelling [1, 2, 6]. Two different crack path descriptions will be considered in the present analysis:

a) **The crack is normal to the surface.** Indeed, as indicated in the introduction, in numerous works published in the literature [1, 2] the crack is assumed to propagate in the normal direction of the surface in a fretting configuration. For such conditions only, one segment is required for the FEM simulation.

b) **The crack is kinked.** The path is described thanks to three segments provided in Figure 6.b. to approximate the real evolution of the crack propagation. This involves an angle of nearly  $47.5^\circ$  on the surface down to  $0^\circ$  deeper below the interface. This description is more complex to implement but it is also more relevant considering the real crack path evolution.

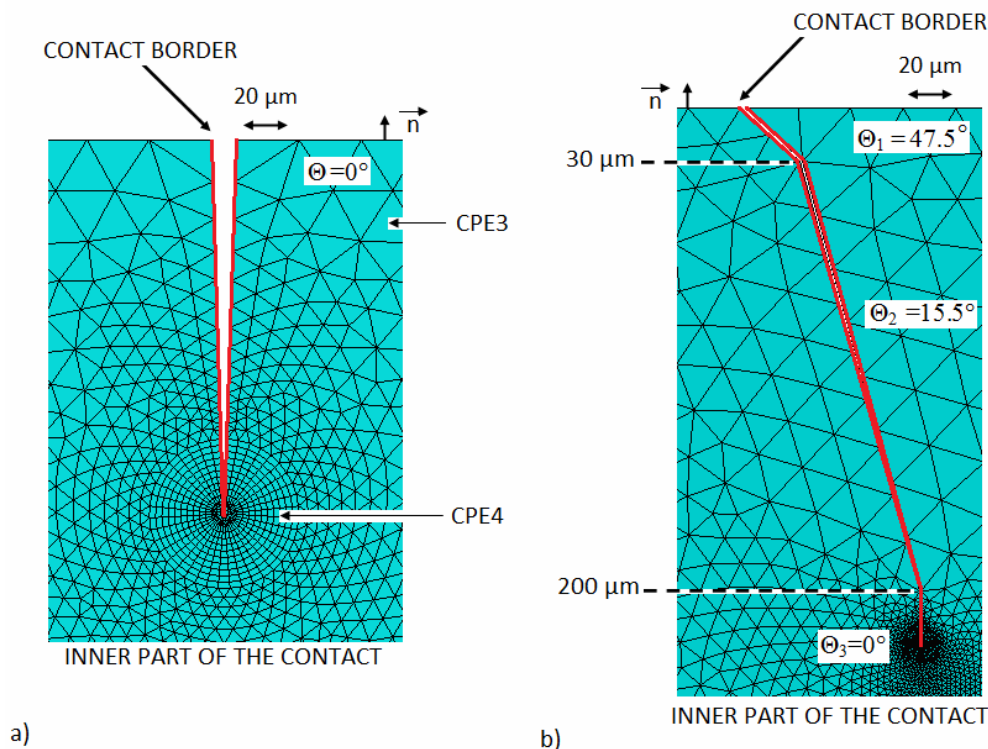


Figure 6. Illustration of the two crack mesh developed in the present investigation a) Plain normal crack hypothesis - b) Kinked crack's description

The Contour Integral's method (CI) is used by Abaqus 6.9 to estimate Stress Intensity Factors (SIF) at the crack tip. First, the Rice's integral (J-integral) is calculated, to then be related to  $K_I$  and  $K_{II}$  [7]. CPE3 triangular elements are used everywhere in the model except for the crack tip, where CPE4 quadrilateral elements are used for the CI. In the present analysis, only the mode I component ( $K_I$ ) will be considered as it is applied in many fretting fatigue modelling description [1]. Although the

model allows us to consider the friction coefficient within the crack lips, in this first analysis, this friction's value (which highly influences the value of the SIF in second mode) is presently assumed to be equal to zero. The stress state below the interface is very complex, to quantify the crack propagation. An effective SIF value based on the ELBER formalism is addressed:

$$\Delta K_{I\text{eff}} = K_{I\text{max}} - 4 \quad \text{for } R > 0$$

$$\Delta K_{I\text{eff}} = K_{I\text{max}} - (4.R + 4) \quad \text{for } -1 < R < 0 \quad \text{with } R = \frac{K_{I\text{min}}}{K_{I\text{max}}}$$

$$\Delta K_{I\text{eff}} = K_{I\text{max}} \quad \text{for } R < -1 \quad (1)$$

An important aspect of this coupled FEM simulation is the fact that the fretting contact description includes the crack's presence in the contact stress analysis. Indeed, the crack can induce a local pressure's and shear's discontinuity at the contact border which will successively modify the contact loading and finally the crack's propagation process (Fig. 7). Note that such coupled interaction between crack and contact stressing is not considered in usual decoupled approaches involving dislocation methods or weight functions [8].

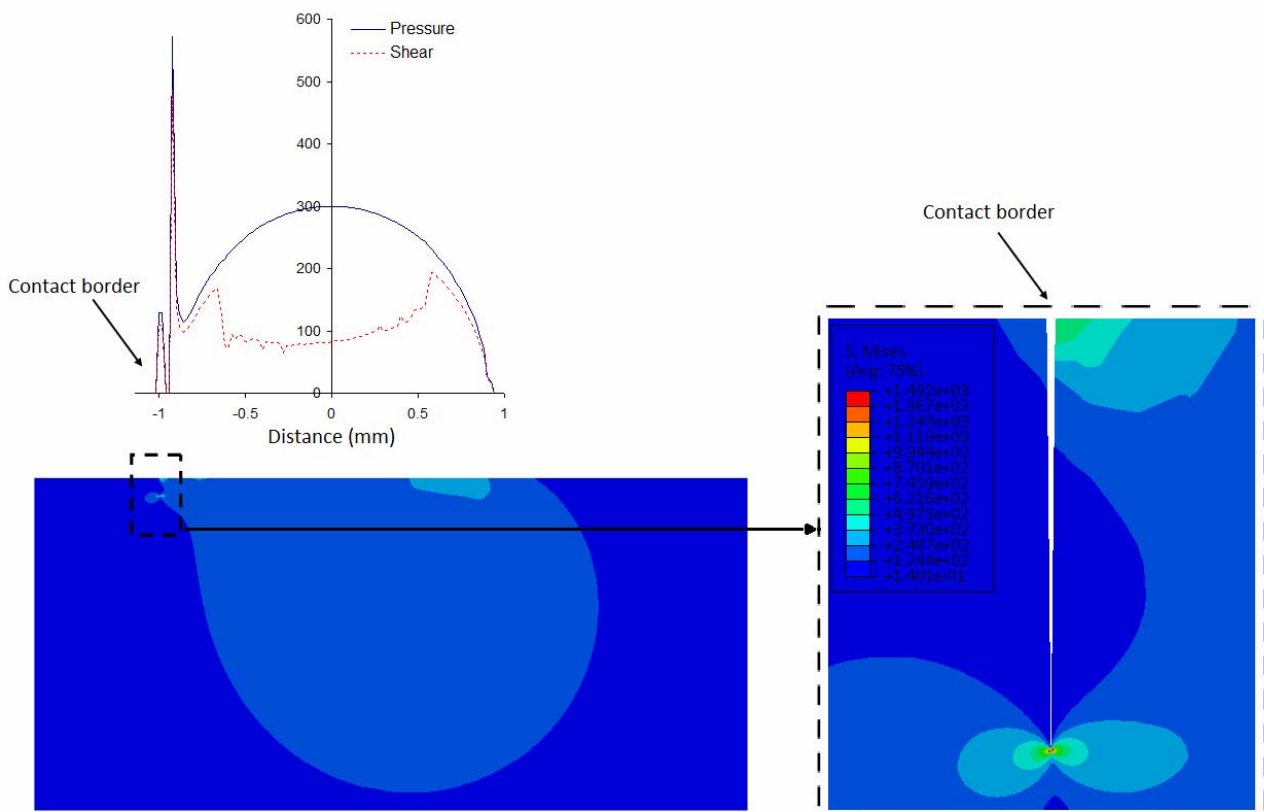


Figure 7. Illustration of the interaction between the contact stress and the crack's presence in the interface ( $Q=Q^*$ , case of a normal crack with  $b_p=100 \mu\text{m}$ )

### 4.3. Results: comparisons between normal and kinked cracks

Figure 8 compares the evolution of the  $K_{I_{max}}$  as a function of the projected crack length obtained for the two crack descriptions.

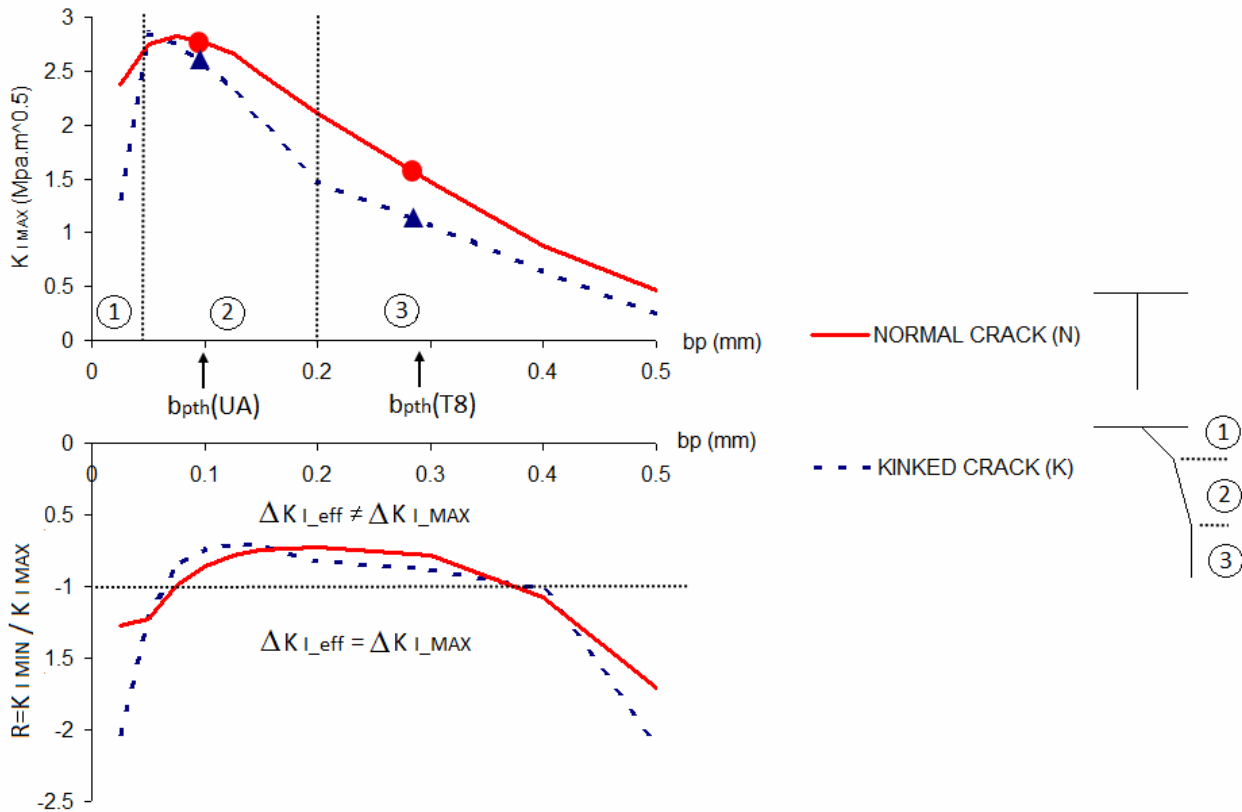


Figure 8. Evolution of the  $K_{I_{max}}$  and R ratio as a function of the projected crack length ( $P=436.5$  N/mm;  $Q=200$  N/mm) computed for the two normal and kinked crack descriptions

Both normal and kinked descriptions lead to similar non monotonic evolutions of the  $K_{I_{max}}$  values. As previously depicted in [9], the  $K_{I_{max}}$  value first increases with the crack length but then decreases when the tip of the crack is more and more remote from the surface due to the very sharp stress decrease induced by the severe contact stress gradients. Focusing on the comparison between kinked and the normal crack path descriptions, it can be said that in the zone 1, next to the surface, the crack angle ( $\Theta_1 = 47^\circ$ ) which is considered in the kinked description tends to reduce the mode I SIF value compared the normal crack description (Fig. 8. zone 1). Then, in the deeper zone 2, the angle decreases ( $\Theta_2 = 15.5^\circ$ ) so that the  $K_{I_{max}}$  value extrapolated from the kinked description is becoming closer to one defined from the normal crack approximation. Finally, in the very deep region 3, the crack orientation turns to the normal direction ( $\Theta_3 = 0^\circ$ ), however the  $K_{I_{max}}$  value provided by the kinked description is still smaller than the value extrapolated using the normal crack description. This difference can be explained by the fact that the lateral position of the crack tip is not the same. Indeed, if the crack tip is still at the vertical of the contact border for the normal crack description, it is now located in the inner compressive part of the contact for the kinked description. A major conclusion of this comparison is the fact that the two approximations of the crack path are in fact rather close. Note that the gap between the  $K_{I_{max}}$  values tends to decrease in

depth. Beside the normal approximation leads systematically higher  $K_{I_{max}}$  values providing conservative descriptions of the crack propagation's risk. Confirming former analytical analyses [9], it can be concluded that the usual "normal" crack path description provides relevant and conservative estimations of the fretting  $K_{I_{max}}$  evolutions. This result is important because it supports numerous plain fretting and fretting fatigue crack propagation's descriptions given in the literature.

#### 4.4. Identification of the $\Delta K_{th}$ crack arrest value

By reporting the maximum projected crack length  $b_{pth}(T8)$  and  $b_{pth}(UA)$  on the previous graph, it is possible to extrapolate the related  $\Delta K_{I_{th}}$  crack arrest value. Hence assuming the "Normal" crack's description we found:

$$\Delta K_{I_{th\_N}}(T8) = 1.6MPa.\sqrt{m} \quad (R=-0.9) \quad \text{and} \quad \Delta K_{I_{th\_N}}(UA) = 2.7MPa.\sqrt{m} \quad (R=-0.9)$$

Whereas using the "kinked" crack description we obtain:

$$\Delta K_{I_{th\_K}}(T8) = 1.2MPa.\sqrt{m} \quad (R=-0.9) \quad \text{and} \quad \Delta K_{I_{th\_K}}(UA) = 2.6MPa.\sqrt{m} \quad (R=-0.75)$$

The extrapolated values are rather small but quite representative of values for such aluminium alloys. Note that such values come from very low stress ratios (R) conditions, which is quite uncommon in conventional fatigue investigations. Considering the "Normal" crack description, which is usually the case in the literature for fretting fatigue cracking's characterizations, we can compare the obtained values with the ultimate stress values (Fig. 9.).

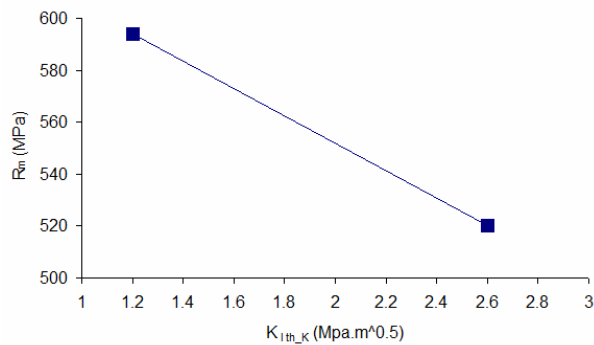


Figure 9. The ultimate stress as a function of  $\Delta K_{th}$

We confirm that for a given alloy, a heat treatment inducing an increase of the ultimate stress, leads to a decrease of the  $\Delta K_{I_{th}}$ . Further developments will consist in comparing the  $\Delta K_{I_{th}}$  identified from this inverse fretting identification's approach with conventional crack propagation fatigue analysis, thus to evaluate the pertinence of this approach and to estimate how very low stress R ratios can be considered regarding the crack arrest process. Besides, mixed mode descriptions including the mode II contribution and the friction coefficient in the crack lips will be addressed.

## 5. Conclusion

Using this reverse analysis, the  $\Delta K_{I_{th}}$  values related to two different microstructures of a similar

Al-alloy were extrapolated. We confirmed that a heat-treatment inducing higher ultimate stresses leads to lower crack arrest stress intensity factors. This investigation underlines that despite its simplicity, a normal description of the fretting crack propagation path provides relevant and above all conservative estimations of the maximum Stress Intensity Factor ( $K_{I_{max}}$ ). In the present work, plain fretting conditions involving very low R ratios (close to -1 or inferior) and a basic mode I description were considered. Besides the effect of the microstructure relate to the multi-crack process is not considered [10]. Future developments will consist in investigating fretting fatigue and fretting on pre-stressed specimen to consider higher R ratio and by implementing a mixed-mode [11] description of the SIF taking into account the coefficient of friction which is operating between the crack edges during the unloading compressive stage.

### Acknowledgements

The authors want to thank the Carnot institute (I@L) for the partial financial support of this research and Constellium CRV company for the furnishing of material specimens.

### References

- [1] J.A. Araújo, D. Nowell, Analysis of pad size effects in fretting fatigue using short crack arrest methodology, *International Journal of Fatigue*, 21 (1999) 947–956.
- [2] S. Fouvry, K. Kubiak, Development of a fretting–fatigue mapping concept: The effect of material properties and surface treatments, *Wear*, 267(2009) 2186–2199
- [3] S. Heredia, S. Fouvry, Introduction of a new sliding regime criterion to quantify partial, mixed and gross slip fretting regimes: Correlation with wear and cracking processes, *Wear*, 269, Issues 7-8, (2010) 515-524.
- [4] J. Delacroix, Etude des Mécanismes de Fissuration en Fatigue et/ou Fretting d'Alliages Al-Cu-Li, PhD, thesis, Institut National des Sciences Appliquées de Lyon, 2011.
- [5] H. Proudhon, S. Basseville, Finite element analysis of fretting crack propagation, *Engineering Fracture Mechanics*, 78 (2011) 685-694.
- [6] H. Proudhon, S. Fouvry, J-Y Buffiere, “Characterisation of fretting fatigue damage using synchrotron X-ray micro-tomography”, *Tribology International* 39 (2006) 1106–1113.
- [7] J.R. Rice, A path independent integral and the approximate analysis of strain concentration by notches and cracks, *Journal of Applied Mechanics*, 35, (1968) 379-386.
- [8] H.F. Bueckner, A novel principle for the computation of stress intensity factors, *Zeitschrift für Angewandte Mathematik und Mechanik*, 50 (1970) 529-546.
- [9] S. Fouvry, D. Nowell, K. Kubiak and D.A. Hills, Prediction of fretting crack propagation based on a short crack methodology, *Engineering Fracture Mechanics*, 75, Issue 6, (2008) 1605-1622.
- [10] J. Delacroix, S. Cazottes, A. Daniélou, S. Fouvry, J.Y. Buffière, Influence of microstructure on the fretting resistance of Al-Cu-Li alloys, ICAA13 13th International Conference on Aluminium Alloys, 2012.
- [11] M.C. Dubourg, A. Chateauminois Experimental and theoretical investigation of the contact fatigue behaviour of an epoxy polymer under small amplitude sliding micro-motions, *European Structural Integrity Society*, 32 (2003) 51-62.